



Evaluation of the Cracking Risk in Alkali Activated Materials by Means of Restrained Shrinkage

Marco Sirotti^(✉), Sarah Blomart, Brice Delsaute, and Stéphanie Staquet

BATir Department, ULB – Université Libre de Bruxelles, CP194/04, 50 Avenue F.D. Roosevelt,
1050 Brussels, Belgium
marco.sirotti@ulb.be

Abstract. Early age micro-cracks development is the source of many durability issues of concrete structures. Specifically, crack formation caused by restrained deformation takes place at a time when the properties of the material are still evolving and its deformation rate is high. The present study used the ring test to investigate the early age cracking sensitivity in restrained conditions of NaOH activated slag. In addition, several parameters were considered, such as the molarity of the activating solution, and the solution-to-binder ratio. An increase in the solution molarity leads to higher compressive strength, autogenous shrinkage, and internal stress, while increasing the solution quantity produces the opposite effect: compressive strength, autogenous shrinkage, and internal stress decrease. Moreover, the internal stress has been compared with the tensile strength of the material showing a good agreement between experimental and modelled results and the low influence of viscous properties of the material at early age. From a general perspective, it has been observed that autogenous shrinkage is the main phenomenon influencing the early age cracking behaviour of alkali-activated slag, whereas creep does not act significantly as a relaxation factor and reduces the internal stress and strain, and the cracking risk.

Keywords: Alkali-activated blast furnace slag · Sodium hydroxide · Restrained shrinkage · Autogenous shrinkage · Microcracks · Creep

1 Introduction

Ground-granulated blast furnace slag represents one of the most promising alternative to Ordinary Portland Cement (OPC), especially for its reduced CO₂ emissions [1–4]. Specifically, alkali-activated slag (AAS) presents interesting performances, such as low permeability, and high strength [5–7]. On the other hand, AAS still raises concerns for its high shrinkage, efflorescence formation, fast carbonation, and cracking tendency [5, 6, 8] which can compromise its durability.

In general, cracks appear when the stress caused by internal or external forces becomes greater than the strength of the material itself. In absence of external forces acting on the material, the main sources of stress for cementitious materials are thermal

deformations and shrinkage, in both autogenous and drying conditions. Thermal deformations are usually associated with the exothermic reaction taking place in the material, while shrinkage depends, among other factors, on the water content of the material. The tests on restrained shrinkage allow to investigate the cracking sensitivity at early age in restrained conditions, trying to reproduce real life situations. In order to do so, several methodologies have been developed where the shrinkage of the sample is mechanically restrained, provoking tensile stresses and subsequent cracking [9].

In the domain of alkali-activated materials, the scarce existing literature on crack formation shows contradictory results. For instance, the studies from Collins and Sanjayan, and Schuab [10, 11] show that AAS in drying conditions presents faster and stronger cracking when compared to OPC. On the other hand, two works from Li *et al.* [12, 13] in autogenous conditions show a different behaviour: regardless of the higher autogenous shrinkage, AAS presents a lower internal stress due to creep and relaxation, causing cracking to appear at a later age. In all the cited cases, the slag activation was carried out using a mixture of sodium silicate and sodium hydroxide, which presents good mechanical properties but in turn has a higher shrinkage if compared with other commonly available activators.

This study aims at understanding the cracking behaviour of NaOH-activated slag using the standard ring test ASTM C1581/C1581M-09 coupled with autogenous shrinkage data from [14]. Specifically, four compositions were tested with two different molarities (2 and 8 M) and two different solution-to-binder (s/b) ratios of 0.5 and 0.8 in order to understand how increasing the quantity of activator affects the behaviour of the material in sealed conditions.

In addition to the experimental ring test, the stress-strain relationship at the external circumference of the mortar sample has been computed using the elastic equations developed by Kovler *et al.* [15]:

$$\sigma_r = -\frac{E}{r^2} \cdot \int_{r_{int}}^{r_{ext}} \varepsilon_{sh} \cdot r \cdot dr + \frac{E \cdot C_1}{2(1-\mu)} - \frac{E \cdot C_2}{(1+\mu)} \cdot \frac{1}{r^2} \quad (1)$$

$$\sigma_r = -\frac{E}{r^2} \cdot \int_{r_{int}}^{r_{ext}} \varepsilon_{sh} \cdot r \cdot dr + \frac{E \cdot C_1}{2(1-\mu)} - \frac{E \cdot C_2}{(1+\mu)} \cdot \frac{1}{r^2} \quad (2)$$

where σ_r is the radial stress, E the E modulus from [16], r the ring radius, r_{int} and r_{ext} the internal and external radius of the mortar specimen respectively, ε_{sh} the autogenous shrinkage deformation, μ the Poisson's ratio from [16], and σ_θ the tangential stress. C_1 and C_2 are two constants obtained considering the boundary conditions $\sigma_r = q_1$ at $r = r_{int}$ and $\sigma_r = q_2$ at $r = r_{ext}$, where q_1 and q_2 are the internal and external surface pressure stress respectively. Equations 1 and 2 do not include creep.

2 Experimental Program

2.1 Materials

The present study investigates the properties of ground granulated blast furnace slag with the oxide composition shown in Table 1. The slag has been combined with different sodium hydroxide solutions with molarities of 2 and 8. The activating solutions have

been prepared by dissolving NaOH pellets into distilled water and stored in airtight containers for 24 h before casting.

Table 1. Oxide composition of the slag.

Oxide	SiO ₂	Al ₂ O ₃	Fe ₂ O ₃	CaO	MgO	K ₂ O
Content [%]	36.2	12.4	0.6	39.8	7.3	0.5

Table 2. Mortar mix proportions.

Composition	s/b ratio	NaOH concentration [M]	Sand-to-paste ratio
S05M2	0.5	2	1
S05M8		8	
S08M2	0.8	2	
S08M8		8	

2.2 Mixing Proportions and Sample Preparation

Four different compositions have been studied and the mixing proportions are summarised in Table 2. All tests have been performed at the mortar scale with a mass sand-to-paste ratio of 1:1, where paste includes both slag and NaOH solution. The reduction of sand content compared to standard OPC is due to strong workability issues in high molarity conditions. The sand was oven dried at 105 °C for 24 h and stored in airtight containers for an additional 24 h before casting.

The different compositions consider two molarities for the sodium hydroxide solution and two different solution-to-binder ratios in order to understand the effect of water content on the cracking properties of AAS.

The mixing has been performed according to the European Standard EN 196–1:1987.

2.3 Methods

Compressive Strength. Cubic samples of 50 mm side were cast, sealed with plastic, and stored in a climatic chamber at 20 ± 0.5 °C. Two samples per composition have been tested at an age of 3, 7, and 24 days using a hydraulic press with accuracy of 1 kN, according to ASTM C109M-13. The results have been compared with previous studies in order to verify the mixing was correct.

Flexural and Compressive Strength. Prismatic samples with dimensions $40 \times 40 \times 160$ mm³ have been tested at an age of 8, 15, and 24 h for flexural and compressive strength at early age. Three samples per composition were tested to ensure proper repeatability.

Restrained Shrinkage. The restrained shrinkage was evaluated using a circular ring test, according to ASTM C 1581:2004. The tests were carried out in sealed conditions at

20 ± 0.5 °C. The sealing was ensured by a double layer of aluminium foil on all sides of the samples. Concerning the geometry, the inner radius of the samples was 152.5 mm, the outer one 190.5 mm and the height 150 mm.

3 Results and Discussion

3.1 Flexural and Compressive Strength

Figure 1 shows the relationship between flexural and compressive strength, which exhibits a linear trend for all compositions. It is evident that increasing the molarity increases the mechanical properties while increasing the s/b ratio produces the opposite effect.

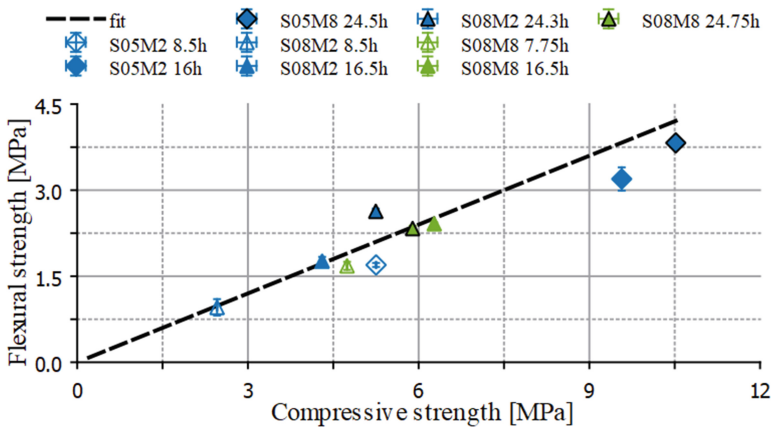


Fig. 1. Flexural vs compressive strength.

3.2 Free Shrinkage

For the data analysis of the ring test results, the evolution of the free shrinkage is essential. In this case, the data for all the compositions was provided by Lacante *et al.* [14] at the paste scale, which were in turn adapted to the mortar compositions used for the ring test. More specifically, the effect of the aggregate has been considered using the following equation:

$$\frac{\varepsilon_m}{\varepsilon_{cp}} = (1 - V_a)^{\eta_{au}} \quad (3)$$

where ε_m is the autogenous strain at the mortar scale, ε_{cp} the autogenous shrinkage at the paste scale, V_a the aggregate content equal to 0.5, and η_{au} the restraining factor. For the restraining factor η_{au} , two boundary conditions of 1.24 and 1.69 were considered based on OPC with w/c ratio = 0.5 and a OPC-BBFS mixture respectively [17]. In particular, an average of the two proved to be in good agreement with what was observed during the ring test itself.

3.3 Restrained Shrinkage

Figure 2 shows the results from the ring test in sealed conditions. In particular, Fig. 2a shows the two compositions with 0.5 s/b and Fig. 2b the two with s/b equal to 0.8. An increase of the solution-to-binder ratio reduced the cracking risk as none of the samples has cracked during the 600 h or more of test. Moreover, the higher amount of solution leads to a reduction of the maximal strain, especially for S08M8. The observations agree with the autogenous shrinkage results for which a decrease in the strain has been observed when the amount of solution was increased [14].

Focusing on Fig. 2a, increasing the molarity from 2 to 8 led to a later age of cracking with a higher maximum strain. Moreover, the molarity increase accelerates the positive strain peak due to the heat release. On the other hand, in 0.8 s/b compositions, the increase in molarity led to a reduction in the strain and an increase of the heat release peak, in agreement with what was observed by Gijbels *et al.* [18].

3.4 Computed Strain

Using Eq. (1) and the autogenous shrinkage for mortar, it is possible to compute the strain in the steel in order to compare it with the gauge values. Figure 3 and Fig. 4 show the comparison for s/b ratio of 0.5 and 0.8 respectively.

For the 0.5 s/b compositions, it is possible to notice that there is a good agreement for S05M2, while the computed strain for S05M8 is way higher than the experimental one, possibly due to relaxation; the results are in line with what observed for OPC, for which creep increases with the amount of water of the mix [17, 19]. On the other hand, the computed curve for S08M8 shows initial shrinkage followed by swelling and shrinkage again, while the experimental curves present an initial swelling followed by shrinkage. The possible explanation is that the model does not describe properly the temperature deformation caused by the high heat release of this composition, but, on the other hand, the autogenous shrinkage values themselves present swelling totally unrelated to the temperature change in the sample [14].

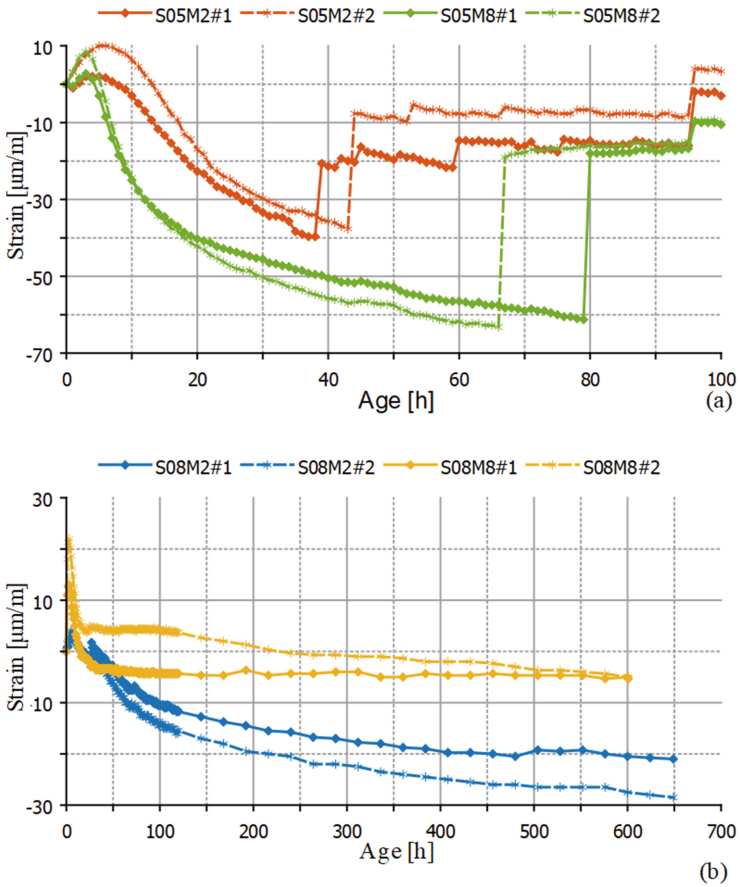


Fig. 2. Ring test comparison in sealed conditions for 0.5 (a) and 0.8 (b) s/b ratio.

3.5 Cracking Time

Cracking takes place when the tensile stress in the sample is higher than its strength. In Fig. 5, the cracking time is compared to the computed strain development and strength. It is important to point out that the flexural strength values have been partially obtained from compressive strength results on cubes of 50 mm side [16] using the linear relationship shown in Fig. 1.

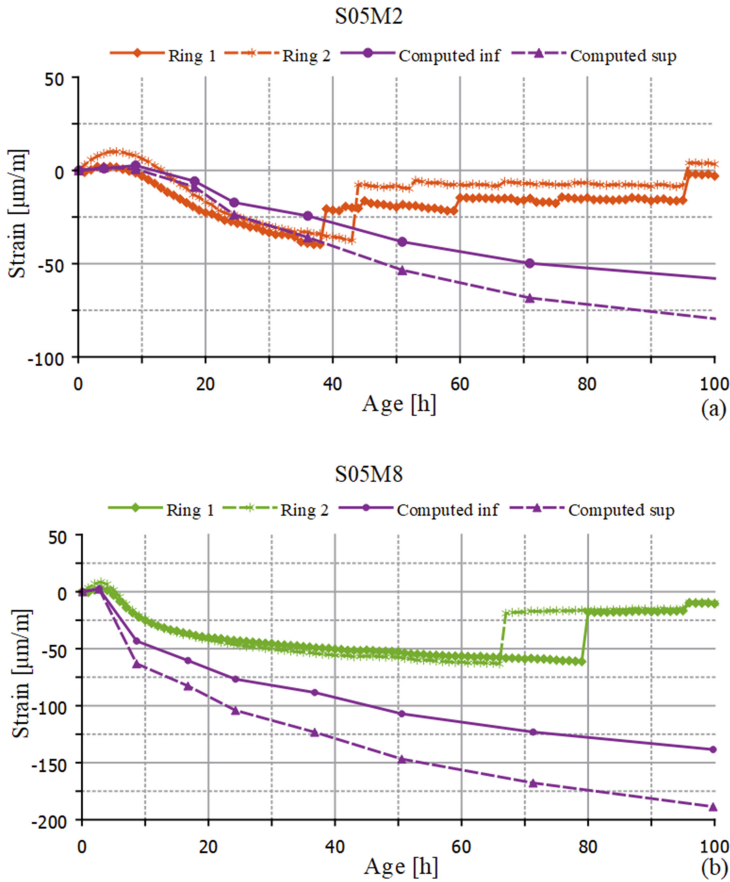


Fig. 3. Comparison between the computed and experimental steel strain for S05M2 (a) and S05M8 (b).

It is possible to notice how the computation describes pretty well the cracking of the 2 molar composition; on the other hand, the 8 molar composition should crack after around 5 h from casting but the experimental results show that it does not happen before more or less 72 h. Said discrepancy can be due to an overestimation of the stress in the modelling phase as the viscous properties of the mortar (creep and relaxation) are not included in the calculation.

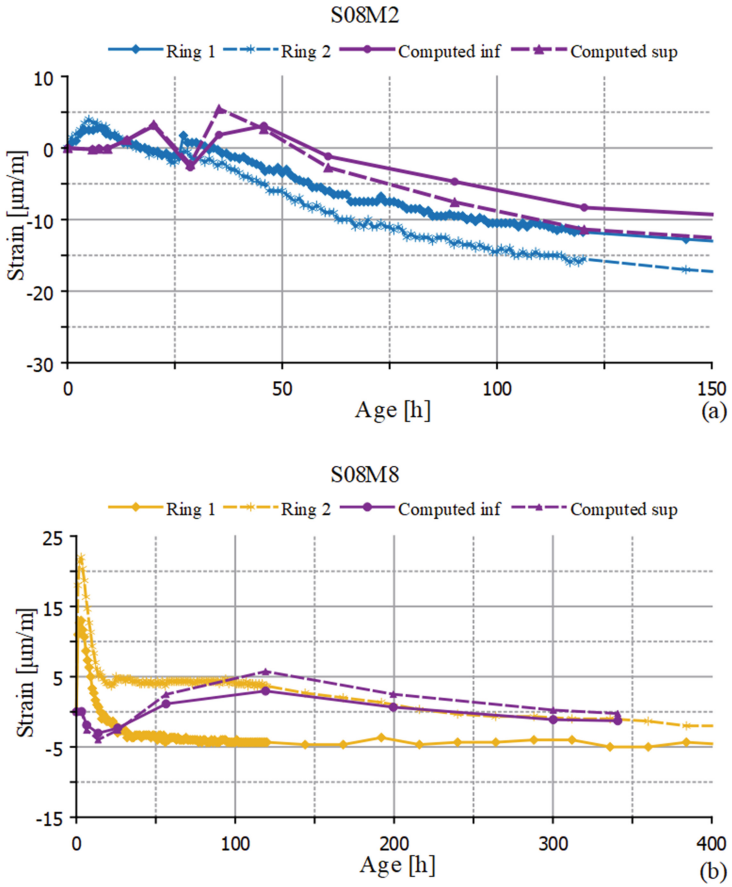


Fig. 4. Comparison between the computed and experimental steel strain for S08M2 (a) and S08M8 (b).

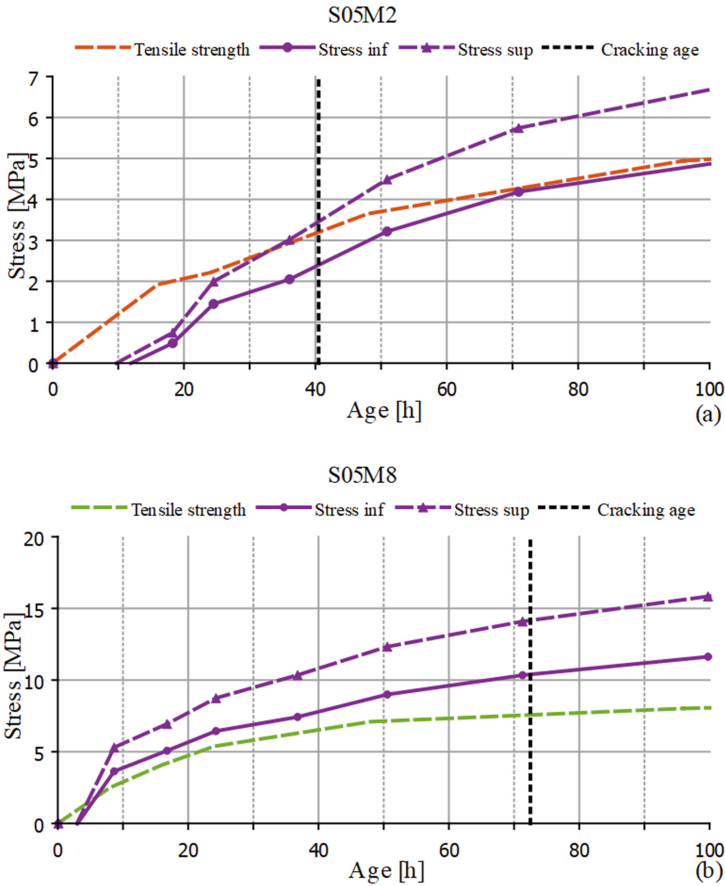


Fig. 5. Comparison between the cracking time and computed stress development and flexural strength for S05M2 (a) and S05M8 (b).

4 Conclusions

In this paper, the cracking tendency of four different alkali-activated slag mortars was studied, alongside with the internal and tangential stress experienced by the material. Based on the results obtained, it is possible to draw the following conclusions:

1. Increasing the molarity, the mechanical properties of alkali-activated slag improve, while increasing the *s/b* ratio, the increased water amount reduces compressive and flexural strength.
2. Increasing the solution-to-binder ratio from 0.5 to 0.8 reduces the stress experienced by the mortar and therefore both cracking risk and strain.
3. Increasing the molarity from 2 to 8 leads to different results according to the *s/b* ratio; if the *s/b* ratio is low, the 8M composition presents higher maximum strain and lower cracking risk, if the *s/b* ratio is higher, the 8M composition shows a lower strain

(swelling), while the cracking risk does not change as no cracks appeared during the first 600 h of test.

4. The elastic strain modelling shows a good agreement with the experimental results for 0.5 solution-to-binder ratio, while the same is not true when increasing it to 0.8, which highlights the importance of creep for compositions with high s/b ratio.
5. The cracking time prediction has high accuracy for S05M2, while, for high molarity, the failure takes place for stress lower of around 60%.
6. From the modelling results it is possible to infer that the viscoelastic properties of the material are low during the first hours of the test as the model considers the sole elastic analysis.

As the study was performed in sealed conditions only, it would be interesting to investigate the effect of environmental conditions on the cracking properties of the material, in order to simulate on site conditions.

Acknowledgements. This paper is the result of research actions performed in the framework of the FNRS-FWO-EOS project 30439691 ‘INTERdisciplinary multiscale Assessment of a new generation of Concrete with alkali-activated maTerials’ (INTERACT). The financial support by FNRS-FWO-EOS is gratefully acknowledged. The authors also want to acknowledge and thank Maité Lacante and Ali Naqi for sharing their results on autogenous shrinkage and mechanical properties of alkali-activated slag and made possible the present study.

References

1. Turner, L.K., Collins, F.G.: Carbon dioxide equivalent (CO₂-e) emissions: a comparison between geopolymers and OPC cement concrete. *Constr. Build. Mater.* **43**, 125–130 (2013). <https://doi.org/10.1016/j.conbuildmat.2013.01.023>
2. Benhelal, E., Zahedi, G., Shamsaei, E., Bahadori, A.: Global strategies and potentials to curb CO₂ emissions in cement industry. *J. Clean. Prod.* **51**, 142–161 (2013). <https://doi.org/10.1016/j.jclepro.2012.10.049>
3. Naqi, A., Jang, J.G.: Recent progress in green cement technology utilizing low-carbon emission fuels and raw materials: a review. *Sustainability* **11**, 537 (2019). <https://doi.org/10.3390/su11020537>
4. Scrivener, K.L., Kirkpatrick, R.J.: Innovation in use and research on cementitious material. *Cem. Concr. Res.* **38**, 128–136 (2008). <https://doi.org/10.1016/j.cemconres.2007.09.025>
5. Ye, H., Cartwright, C., Rajabipour, F., Radlińska, A.: Understanding the drying shrinkage performance of alkali-activated slag mortars. *Cement Concr. Compos.* **76**, 13–24 (2017). <https://doi.org/10.1016/j.cemconcomp.2016.11.010>
6. Juenger, M.C.G., Winnefeld, F., Provis, J.L., Ideker, J.H.: Advances in alternative cementitious binders. *Cem. Concr. Res.* **41**, 1232–1243 (2011). <https://doi.org/10.1016/j.cemconres.2010.11.012>
7. Wang, S.-D., Pu, X.-C., Scrivener, K.L., Pratt, P.L.: Alkali-activated slag cement and concrete: a review of properties and problems. *Adv. Cem. Res.* **7**, 93–102 (1995). <https://doi.org/10.1680/acr.1995.7.27.93>
8. Ye, H., Cartwright, C., Rajabipour, F., Radlińska, A.: Effect of Drying Rate on Shrinkage of Alkali-Activated Slag Cements. In: *International Conference on Durability of Concrete Structures* (2014)

9. Delsaute, B., Staquet, S.: Testing concrete since setting time under free and restrained conditions. In: Serdar, M., Gabrijel, I., Schlicke, D., Staquet, S., Azenha, M., editors. *Advanced Techniques for Testing of Cement-Based Materials*, Cham: Springer International Publishing; 2020, pp. 177–209. https://doi.org/10.1007/978-3-030-39738-8_6
10. Collins, F., Sanjayan, J.G.: Cracking tendency of alkali-activated slag concrete subjected to restrained shrinkage. *Cement and Concrete Research* 2000:8
11. Schuab, M.R.: On the development of MK/BFS alkali-activated materials as repair mortars: Performance under free and restrained shrinkage tests. *Construction and Building Materials* 2021:14
12. Li, Z., Zhang, S., Liang, X., Ye, G.: Cracking potential of alkali-activated slag and fly ash concrete subjected to restrained autogenous shrinkage. *Cement Concr. Compos.* **114**, 103767 (2020)
13. Li, Z., Delsaute, B., Lu, T., Kostiuhenko, A., Staquet, S., Ye, G.: A comparative study on the mechanical properties, autogenous shrinkage and cracking proneness of alkali-activated concrete and ordinary Portland cement concrete. *Construct. Build. Mater.* 292, 123418 (2021)
14. Lacante, M., Delsaute, B., Staquet, S.: Effect of internal and external factors on the volume changes of slag binder activated by sodium hydroxide at early-age, Milos (Greece): (2023)
15. Kovler, K., Sikuler, J., Bentur, A.: Restrained shrinkage tests of fibre-reinforced concrete ring specimens: effect of core thermal expansion. *Mater. Struct.* **26**, 231–237 (1993). <https://doi.org/10.1007/BF02472616>
16. Naqi, A., Delsaute, B., Königsberger, M., Staquet, S.: Monitoring and modelling of visco-elastic strains of alkali-activated slag mortar since the earliest age, Milos (Greece): (2023)
17. Delsaute, B.: New approach for Monitoring and Modelling of the Creep and Shrinkage behaviour of Cement Pastes. Université Libre de Bruxelles (ULB), *Mortars and Concretes since Setting Time* (2016)
18. Gijbels, K., Pontikes, Y., Samyn, P., Schreurs, S., Schroevers, W.: Effect of NaOH content on hydration, mineralogy, porosity and strength in alkali/sulfate-activated binders from ground granulated blast furnace slag and phosphogypsum. *Cem. Concr. Res.* **132**, 106054 (2020). <https://doi.org/10.1016/j.cemconres.2020.106054>
19. Le Roy, R.: *Déformations instantanées et différées des bétons à hautes performances* (1995)